Science of the Total Environment 851 (2022) 158082

Contents lists available at ScienceDirect

Science of the Total Environment

journal homepage: www.elsevier.com/locate/scitotenv

Suppression of the phenolic SOA formation in the presence of electrolytic inorganic seed

Jiwon Choi, Myoseon Jang *

Department of Environmental Engineering Sciences, University of Florida, Gainesville, FL 32611, USA

HIGHLIGHTS

- SOA formation from the photooxidation of phenol and *o*-cresol.
- Ozone depletion caused by heterogeneously formed phenoxy radicals.
- Prediction of SOA formation via multiphase reactions of phenolic hydrocarbons.

GRAPHICAL ABSTRACT

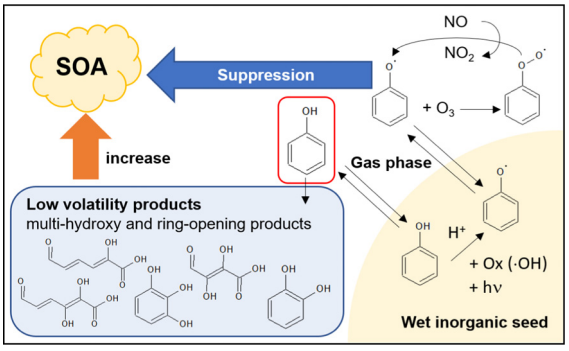

ARTICLE INFO

Editor: Pingqing Fu

Keywords:
Phenol
Cresol
SOA
Photooxidation

ABSTRACT

Phenolic compounds are largely attributed to wildfire gases and rapidly react with atmospheric oxidants to form persistent phenoxy free radicals, which influence atmospheric chemistry and secondary organic aerosol (SOA) formation. In this study, phenol or *o*-cresol was photochemically oxidized under various conditions (NO_x levels, humidity, and seed conditions) in an outdoor photochemical reactor. Unexpectedly, SOA growth of both phenols was suppressed in the presence of salted aqueous aerosol compared to non-seed SOA. This discovery is different from the typical SOA formation of aromatic or biogenic hydrocarbons, which show noticeably higher SOA yields via organic aqueous reactions. Phenol, *o*-cresol, and their phenolic products (e.g., catechols) are absorbed in aqueous aerosol and form phenoxy radicals via heterogeneous reactions under sunlight. The resulting phenoxy radicals are redistributed between the gas and particle phases. Gaseous phenoxy radicals quickly react with ozone to form phenyl peroxide radicals and regenerated through a NO_x cycle to retard phenol oxidation and SOA formation. The explicit oxidation mechanisms of phenol or *o*-cresol in the absence of aqueous phase were derived including the Master Chemical Mechanism (MCM v3.3.1) and the path for peroxy radical adducts originating from the addition of an OH radical to phenols to form low volatility products (e.g., multi-hydroxy aromatics). The resulting gas mechanisms of phenol or *o*-cresol were, then, applied to the Unified Partitioning Aerosol Phase Reaction (UNIPAR) model to predict SOA formation via multiphase partitioning of organics and aerosol-phase oligomerization. The model well simulated chamber-generated phenolic SOA in absence of wet-inorganic seed, but significantly overestimated SOA mass in presence of wet seed. This study suggests that heterogeneous chemistry to form phenoxy radicals needs to be included to improve SOA prediction from phenols. The suppression of atmospheric oxidation due to phenoxy radicals in wet inorganic aerosol can explain the low SOA formation during wildfire episodes.

* Corresponding author.
E-mail address: mjang@ufl.edu (M. Jang).

http://dx.doi.org/10.1016/j.scitotenv.2022.158082
Received 27 April 2022; Received in revised form 28 July 2022; Accepted 12 August 2022
Available online 17 August 2022

1. Introduction

Organic matter (OM) is a major constituent ranging from 20 % to 90 % of fine particulate matter mass (Jimenez et al., 2009; Zhang et al., 2007). Secondary organic aerosol (SOA) forms through the atmospheric oxidation of hydrocarbons (HCs) emitted from anthropogenic activities and vegetation (Finlayson-Pitts and Pitts, 1999) and constitutes a significant portion of tropospheric OM (on average 40 % to 90 %) (Kleindienst et al., 2007; Docherty et al., 2008; Mancilla et al., 2015). SOA has been extensively studied due to its influence on climate forcing (Hallquist et al., 2009; Steinfeld, 1998) or adverse health effects (Pope Iii et al., 2002; Cohen et al., 2017).

Recently, biomass burning has received large attention because of increasing occurrences of wildfires and continuous agricultural burning. The global mean fire weather season length increased by 18.7 % from 1979 to 2013 and the global frequency of long fire weather seasons increased by 53.4 % during 1996–2013, compared with 1979–1996 (Jolly et al., 2015). For example, a megafire across Victoria, Australia burned 1.5 million hectares during 2019–2020 compared to 211,713 ha burned during 2018–2019 (Lindenmayer and Taylor, 2020). Furthermore, many developing countries adopt agricultural burning for farming such as China, India, and countries in South Asia, Africa, and South America (Yevich and Logan, 2003; Chen et al., 2017; Jethva et al., 2018; Johnson et al., 2008; Permadi and Oanh, 2013). During biomass burning, various volatile organic compounds (VOCs) and intermediate volatile organic compounds (IVOCs) capable of producing SOA are emitted to the tropospheric atmosphere (Kelly et al., 2018). Among SOA precursors, phenolic compounds account for a large portion of biomass burning-driven SOA mass (Majdi et al., 2019). In a study by (Bruns et al., 2016), the SOA associated with phenolic compounds attributes to over 30 % of total wood smoke SOA and 50 % of the SOA mass among identified VOCs and IVOCs. Akherati et al. reported in their chamber study that phenols contribute to 20 % of the total VOC and IVOC emissions in biomass burning gases and comprise nearly 60 % of total SOA mass. Furthermore, phenol, cresol, and catechol account for >50 % of SOA formation (Akherati et al., 2020) in biomass burning smoke.

The SOA formation potential from phenolic compounds (Akherati et al., 2020) is generally larger than that from the conventional SOA precursor HCs, such as, biogenic VOCs and aromatic VOCs (Ng et al., 2007; Smith et al., 2014). However, field data shows an insignificant change in organic aerosol mass during wildfire events. For example, Hodshire et al. reported increases in organic aerosol mass with age of biomass burning smoke while they observed no net change in aerosol mass with age in field data (Hodshire et al., 2019). In addition to little SOA growth, several papers reported even a net loss of organic aerosol mass (Capes et al., 2008; May et al., 2015). Considering dominance of phenols in biomass burning smoke gases, such a discrepancy between laboratory studies and field data possibly can be explained by unidentified mechanisms in atmospheric oxidation of phenols (Nakao et al., 2011; Carter et al., 2012; Yu et al., 2016). Challenges to the prediction of phenolic SOA formation include imperfect gas-phase oxidation mechanisms and heterogeneous chemistry of oxidized products in aerosol phase.

Gaseous phenols rapidly react with OH radicals and they can form phenoxy radicals, which is monovalent oxygen radical species and delocalized over the aromatic ring.

$$C_6H_5OH + OH \rightarrow C_6H_5O\cdot \quad (1)$$

Unlike aliphatic alkoxy radicals that can react with an oxygen molecule to form an HO_2 (hydroperoxyl) radical, phenoxy radicals have resonance stability via aromaticity and no aliphatic hydrogen at the carbon attached to O-radical. Therefore, the lifetime of phenoxy radicals is relatively long in ambient air (Spanget-Larsen et al., 2001) and interrupt typical atmospheric chemistry and SOA formation. Furthermore, the laboratory study by Tao and Li (1999) shows a rapid reaction of a phenoxy radical with ozone (in the scale of 10^{-13}) to form phenylperoxide radicals.

$$C_6H_5O\cdot + O_3 \rightarrow C_6H_5OO\cdot \quad (2)$$

$C_6H_5OO\cdot$ reacts with NO to form NO_2 and regenerate $C_6H_5O\cdot$ (Carter and Atkinson, 1989):

$$C_6H_5OO\cdot + NO \rightarrow C_6H_5O\cdot + NO_2 \quad (3)$$

The dramatic reduction of ozone can suppress the OH radical production cause a significant retardation of phenol consumption, and slow down NO decay during the photochemical reaction (Matsumi and Kawasaki, 2003). Additionally, the phenoxy radical can react with the HO_2 radical to form phenol (Jenkin et al., 2018; Platz et al., 1998).

$$C_6H_5O\cdot + HO_2 \rightarrow C_6H_5OH + O_2 \quad (4)$$

The slow phenol decay possibly would suppress SOA growth and the degree of aging. It is contradicted with laboratory data, which shows rapid SOA growth with high SOA yields from the atmospheric oxidation of phenolic compounds (Yee et al., 2013; Smith et al., 2014; Sun et al., 2010; Nakao et al., 2011) add. To date, the formation mechanisms of phenoxy radicals and their significance on atmospheric environments are not well studied.

The multi-generation oxidation of hydrocarbons in gas phase creates highly oxidized, low volatility products possibly to increase SOA mass (Donahue et al., 2012; Yee et al., 2013; Schwantes et al., 2017). Phenols, OH-substituted benzenes, are more reactive than the conventional aromatic hydrocarbons due to phenol OH group's electron receiving characteristics (Hansch et al., 2000). Thus, phenols are highly reactive for the addition of OH radicals into an aromatic ring and easily produce multihydroxybenzenes (Nakao et al., 2011; Yee et al., 2013; Ji et al., 2017; Schwantes et al., 2017).

In addition to gas oxidation, heterogeneous reactions of reactive organic species in aerosol phase can be a significant contributor to SOA burdens in many precursors.(Hallquist et al., 2009) Such chemistry includes condensation reactions between organic compounds (i.e., hemiacetal/acetal formation and aldol condensation), reactions of organics with water (i.e., hydration of aldehydes and hydrolysis of epoxides), and esterification of sulfate with organics (organosulfate formation) (Hallquist et al., 2009; Jang et al., 2002; Surratt et al., 2007). The oligomerization of organic species in aerosol phase is also known to be accelerated by an acid catalyst, such as sulfuric acid, to increase SOA formation (Zhang et al., 2015; Laskin et al., 2018; Jang et al., 2002; Tolocka et al., 2004). In order to predict SOA formation, partitioning base semiempirical models such as the two product model (Odum et al., 1996) and the Volatility-Base Set (VBS) (Donahue et al., 2006) have been employed in regional models because they are relatively simple due to the small number of model parameters (Volkamer et al., 2006; Barsanti et al., 2017; Wang et al., 2015; Zhao et al., 2016). However, oversimplification of partitioning-based models can cause underestimation of SOA formation due to missing aerosol chemistry and gas oxidation products produced with aging. Currently, few models for aerosol chemistry compensate for these shortcomings (Hallquist et al., 2009).

In this study, the SOA formation of phenol or *o*-cresol, which is abundant in wildfire smoke gases, was predicted using the Unified Partitioning Aerosol Phase Reaction (UNIPAR) model. In order to improve volatility-reactivity base lumping array, the UNIPAR model utilizes explicitly predicted gas products, which originated from the Master Chemical Mechanism (MCM v3.3.1) and the new pathways of oxygenated, low volatility products (Schwantes et al., 2017; Pillar-Little et al., 2015; Yee et al., 2013; Yu et al., 2016). The UNIPAR model streamlines multiphase partitioning and aerosol phase reactions in both organic and salted aqueous phases (Yu et al., 2022; Yu et al., 2021b; Han and Jang, 2020; Zhou et al., 2019; Beardsley and Jang, 2016; Im et al., 2014). The suitability of the UNIPAR model was demonstrated by comparing simulation and chamber

data obtained from the photooxidation of phenol or *o*-cresol under various NO_x levels and seed conditions, such as sulfuric acid (SA) or wet-ammonium sulfate (wet-AS) aerosols, in a large outdoor photochemical reactor. The environmental factor to form phenoxy radicals was also investigated under controlled chamber experimental conditions. This study benefits the evaluation of SOA formation with phenols aging at relatively high NO_x levels when biomass burning smoke parcels intrude to the urban atmosphere.

2. Experimental section

2.1. Chamber experiments

To produce phenolic SOA, the University of Florida Atmospheric PHotochemical Outdoor Reactor (UF-APHOR) dual Teflon film chamber (each with 52-m^3 volume and 86-m^2 surface area) is utilized under ambient sunlight. Phenolic SOA was produced from photooxidation of phenol (Acros Organics, 99 %) or *o*-cresol (Sigma-Aldrich, ≥99 %) under different NO_x levels (high NO_x: HC/NO_x < 5 ppbC/ppb and Low NO_x: HC/NO_x > 5 ppbC/ppb) and various inorganic seed conditions (no seeded SOA, SOA with SA, and SOA with AS). A detailed description of the experimental conditions has been described in many previous studies (Beardsley and Jang, 2016; Zhou et al., 2019; Han and Jang, 2020; Yu et al., 2021b). In brief, NO (2 % in N_2, Airgas, USA), HCs, and inorganic seed aerosol were injected into the chamber before sunrise. Hydrocarbons (phenol or *o*-cresol) were vaporized into the chamber using a glass manifold under clean air streams. Phenol or *o*-cresol was collected in 0.1 M NaOH aqueous solution with an impinger at 1 LPM downstream pump. The concentrations of phenol and *o*-cresol were measured with an ultraviolet (UV) spectrometer (Lambda 35, PerkinElmer, CT, USA) at 287 nm and 263 nm, respectively. In NaOH aqueous solution, phenoxides show a much stronger UV absorption than phenols. Non-reactive CCl_4 (Sigma-Aldrich, ≥99.5 %) was also introduced into the chamber to monitor chamber air dilution and its concentration was measured by a Gas Chromatograph with a Flame Ionization Detector (7820A, Agilent Technologies, CA, USA). The concentrations of NO_x and ozone were monitored using a photometric ozone analyzer (Model 106-L, 2B Technologies, MA, USA) and a chemiluminescence NO/NO_x analyzer (Model 405, 2B technologies, MA, USA), respectively. For SA or wet-AS seeded SOA, 0.05 M SA aqueous solution or 0.05 M AS solution was atomized using a nebulizer (LC STAR, PARI, Starnberg, Germany) into the chamber. For dry-AS seeded experiments, RH was controlled below efflorescence relative humidity (ERH), and for wet-AS experiments, RH was maintained above ERH to prevent crystallization of seed.

The particle size distribution and volume concentration were monitored using a Scanning Mobility Particle Sizer (SMPS, TSI model 3080, Shoreview, MN, USA). The intensity of selected ion peaks in aerosol were monitored using an Aerosol Chemical Speciation Monitor (ACSM, Aerodyne Research, Billerica, MA, USA). The concentration of organic carbon (OC) in aerosol was monitored using an Organic Carbon/Elemental Carbon aerosol analyzer (OC/EC Model 4, Sunset Laboratory, Hillsborough, NC, USA). The conversion factor of OC to OM for both phenol SOA and *o*-cresol SOA was 2.2, which was determined by comparing OC data with SOA filter mass. SOA mass was estimated by the weight difference before and after SOA collection on the filter. The aerosol mass was collected on the Teflon film with an acetone-drenched nylon filter and measured with an analytical balance (MX5, Mettler-Toledo Ltd., Columbus, OH). The concentration of water-soluble inorganic species (Sulfate, nitrate, and ammonium ions) was measured by an Ion Chromatograph (Compact IC 761, Metrohm Inc., Switzerland) coupled to a Particle into Liquid Sampler (ADISO 2081, Applikon Inc., USA) (PILS-IC). The proton concentration in acidic aerosol was measured by a Colorimeter coupled with a Reflectance UV–Visible Spectrometer (C-RUV) (Jang et al., 2008; Li and Jang, 2012). All gas data were corrected for chamber air dilution. All aerosol data were corrected for gas dilution and aerosol loss to the chamber wall as done in previous chamber studies (Li et al., 2015; Im et al., 2014; Han and Jang, 2020).

Temperature and relative humidity (RH) inside the chamber were measured using a hygrometer (CR1000 measurement and control system, Campbell Scientific, UT, USA). Sunlight intensity was monitored with a Total UV Radiometer (TUVR, Eppley Laboratory, RI, USA). Time profiles of RH, temperature and sunlight intensity are in Fig. S1. Table 1 summarizes the chamber experimental conditions of this study.

2.2. Aerosol composition measured with Fourier-transform infrared spectroscopy

The functional group distribution of SOA was constructed using spectral data obtained with a Fourier-Transform Infrared (FTIR) Spectrometer (Nicolet iS50, Thermo Fisher Inc., USA). The selected SOA (Table 1) was collected on a silicon disc (13 × 2 mm, Sigma-Aldrich, USA) by impaction using a fabricated sampling holder for 120 min between 1:00 PM and 3:00 PM EST. The FTIR data was obtained immediately after the collection of SOA to avoid the loss of aerosol by evaporation. FTIR spectra was obtained with a (duterated triglycine sulfate (DTGS) detector ranging from 400 cm^{-1} to 4000 cm^{-1} and a resolution of 0.482 cm^{-1} for 32 scans. To

Table 1
Chamber experimental conditions for the photooxidation of phenol and *o*-cresol in the UF-APHOR dual chambers and resulting SOA data.

HC	No.	Date	[a]Initial HC ppb	Initial NO ppb	[b]HC/NOx ppbC/ppb	[c]Seed	Seed mass μg/m3	RH %	Temp K	[d]Mean diameter Nm	[e]ΔHC μg/m^3	[f]SOA mass μg/m^3	Yields	Comments
Phenol	1	09/07/2021	79	85	5.6	None	N.A.	19–45	298–320	191	200	71	0.35	Fig. 4
	2	09/30/2021	115	87	7.3	None	N.A.	16–41	298–321	205	269	112	0.41	Fig. 4 FTIR
	3	10/31/2021	94	99	5.3	Dry-AS	16	19–47	283–299	201	231	69	0.30	Fig. 4
	4	10/31/2021	72	98	4.6	Wet-AS	169	71–97	282–300	217	192	87	0.45	Fig. 5
	5	09/07/2021	130	90	8.0	SA	332	15–56	296–320	244	185	48	0.25	Fig. 5
	6	09/30/2021	174	82	11.7	SA	160	14–46	297–318	223	304	43	0.14	Fig. 5 FTIR
o-Cresol	7	10/14/2021	72	69	6.4	None	N.A.	16–60	292–319	186	318	215	0.65	Fig. 4 FTIR
	8	10/22/2021	58	58	6.3	None	N.A.	15–49	292–315	188	257	167	0.64	Fig. 4
	9	11/17/2021	58	73	5.4	Dry-AS	21	17–54	285–311	255	257	207	0.80	Fig. 4
	10	11/08/2021	48	48	7.0	Wet-AS	145	52–90	278–304	222	212	147	0.69	Fig. 5
	11	10/14/2021	65	63	6.1	SA	214	17–53	293–321	231	106	60	0.56	Fig. 5 FTIR
	12	10/22/2021	47	56	5.2	SA	173	16–40	291–316	235	124	75	0.60	Fig. 5

N.A.: not applicable

[a] The initial HC was collected using a midget impinger filled with 12 mL 0.1 M NaOH aqueous solution by passing the clean air at 1 LPM for 20 min. The collected samples were measured using a UV spectrometer.

[b] High NO_x: HC ppbC/NO_x ppb < 5; low NO_x: HC/NO_x > 5 ppbC/ppbS

[c] The seed condition refers to the injected electrolytic seed: sulfuric acid (SA), wet ammonium sulfate (wet-AS), dry AS (dry-AS).

[d] The reported geometric mean diameters are determined at 4 PM of each experiment. The geometric mean diameter of the initial inorganic seed particle ranges from 93 nm (dry-AS aerosol) 146 (sulfuric acid aerosol) based on SMPS data. The geometric standard deviations range from 1.39 to 1.76.

[e] ΔHC is difference between initial concentration and the concentration at 16 PM.

[f] The SOA mass reported is from OC data at 4:00 PM EST.

collect and process FTIR data, the software Omnic v9 (Thermo Fisher Scientific) was used. The functional group compositions (—OH, —COOH, —C═C, C—O, C═O and —NO_2) of each SOA were constructed by decoupling of the FTIR spectrum as described in previous studies (Zhou et al., 2019; Beardsley et al., 2013).

3. Model description

3.1. SOA formation

The SOA formation via multiphase reaction of phenol or *o*-cresol was simulated with the UNIPAR model. Fig. 1 illustrates the overall scheme of the UNIPAR model. The UNIPAR model was previously described in many papers (Im et al., 2014; Han and Jang, 2020; Yu et al., 2021b; Zhou et al., 2019; Yu et al., 2022). The details of the model are also described in Section S2 of Supporting Information. The separation RH (SRH) values between the organic and inorganic phases in aerosol estimated by integrating aerosol's physicochemcial parameters (i.e., salt compositions, oxygen to carbon ratios, hydrogen-bonding ability, and average moelcular weight) into the mathematical equation recently derived by Yu et al. (2021a). The estimated SRH ranges 0.61 to 0.7 for phenol SOA and 0.68 to 0.76 for cresol SOA. The RH values of this study were mostly below 60 % over the course of the experiment (Table 1). Hence, SOA formation in the presence of salted aqueous phase is assumed to be governed by Liquid-Liquid Phase Separation. In order to provide better gas product distributions, the newly constructed mechanims to produce multi-hydroxybenzenes and their oxidation (Nakao et al., 2011; Schwantes et al., 2017; Yee et al., 2013) were integrated to the MCM (v3.3.1). The oxidized products predicted from the newly constructed explicit mechanisms in gas (*g*) phase were then classified into 50 lumping groups according to their reactivity and volatility. The UNIPAR model streamlines multiphase partitioning, oligomerization in organic phase (*or*) and aqueous reactions in inorganic phase (*in*). For the sensitivity test, the UNIPAR model employs the model parameters free from the artifacts due to gas-wall partitioning to simulate SOA mass in ambient air (Han and Jang, 2020).

3.2. Gas oxidation mechanisms

The atmospheric oxidation of phenol and *o*-cresol was predicted by using near explicit gas mechanisms to produce product distributions that are integrated into the UNIPAR model in Section 3.1. In MCM, the branching ratios to form phenoxy radicals from the reaction of phenols with OH radicals were reduced to improve the prediction of the decay of phenols and atmospheric chemistry of tracers (ozone and NO_x). Further discussion can be seen in Section 4.1 (Impact of Inorganic Seed on Gas Simulation of Phenols) below.

In addition, the explicit model captures the gas mechanisms to form low-volatile multi-hydroxybenzenes from addition of the OH radical to phenol and *o*-cresol (Nakao et al., 2011; Schwantes et al., 2017; Yee et al., 2013). Peroxide compounds and quinone derived from the OH addition to multi-hydroxybenzenes were also included in the explicit mechanisms (Olmez-Hanci and Arslan-Alaton, 2013; Schwantes et al., 2017). The pathways to form these low-volatile products are shown in Figs. S2 and S3 for phenol and *o*-cresol, respectively.

Nakao et al. identified a series of OH addition reactions to catechol by characterizing water soluble gas-phase compounds using a Particle-into-Liquid Sampler and Electrospray Ionizer coupled with an Agilent Time-of-Flight Mass Spectrometer (PILS-ESI-TOFMS) (Nakao et al., 2011). Yee et al. also reported continuous OH addition to phenolic compounds and low-volatile ring opening products from multi-hydroxybenzenes (Yee et al., 2013). Nakao et al. (2011) also tentatively characterized the formation of bicyclic peroxides and further decomposition of products into alkoxy radicals under high NO levels (Atkinson, 2000; Calvert et al., 2002). Laboratory studies show the detection of the quinones from the oxidation of both phenol or *o*-cresol (Olmez-Hanci and Arslan-Alaton, 2013; Schwantes et al., 2017). Sun et al. found that the OH-initiated reactions of phenols formed ring-opening products containing multiple OH groups using a High-Resolution Time-of-Flight Aerosol Mass Spectrometer (HR-AMS) (Sun et al., 2010).

Therefore, following the former study, OH addition mechanisms were added to the MCM to form multi-hydroxybenzenes, peroxy radicals, and quinones and then undergo ring-retaining or ring-opening reactions. As

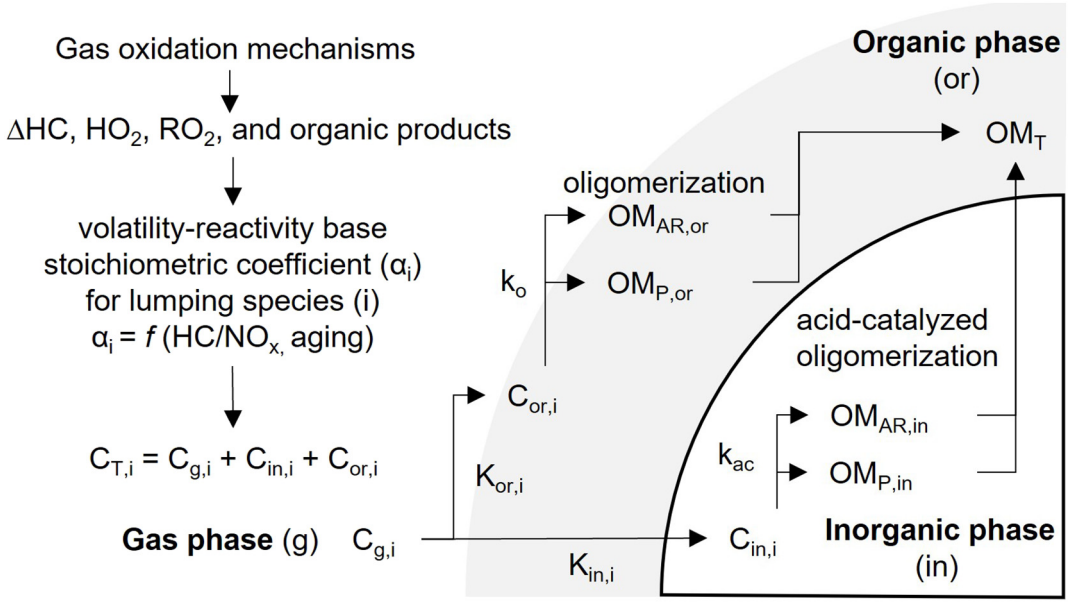

Fig. 1. Scheme of the UNIPAR model. The oxidized products predicted from the explicit gas mechanism (MCM v.3.3.1) are classified into 50 lumping species (*i*) based on volatility and reactivity. The consumption of hydrocarbons (ΔHCs), the concentration of hydroperoxy radical (HO_2), alkylperoxy radical (RO_2), and the organic products are also simulated by using MCM and applied to the UNIPAR model. The lumping array associated with stoichiometric coefficients is dynamically constructed as a function of the HC ppbC/NO_x ratio and the aging scale, which is estimated with the concentrations of HO_2 and RO_2 radicals. "C" denotes the concentration of an organic compound and K denotes partitioning coefficient of an organic compound. Subscripts "g", "or", and "in" represent gas, organic, inorganic phase, respectively. OM refers the organic matter. Subscripts "AR", "P", and "T" refers aerosol-phased reaction, partitioning, and total.

seen in Figs. S2 and S3, fraction d to form non-bicyclic peroxide radicals (the OH addition to phenol followed by the addition of an oxygen molecule) was set to 0.1 based on FTIR data and the prediction of SOA mass from this study. Fraction d was applied to a series of multi-hydroxybenzenes to form non-bicyclic peroxide radicals that can produce low volatile oxidized products. The reaction rate constants for the addition of the OH radical to the newly added phenolic compounds were calculated based on the structure-reactivity relationship (Kwok and Atkinson, 1995).

4. Results and discussion

4.1. Impact of inorganic seed on gas simulation of phenols

Fig. 2 illustrates measured gaseous species (phenol, *o*-cresol, ozone, NO, and NO_2) in the UF-APHOR chamber and simulation results with both the unmodified and modified MCM v3.3.1 mechanisms (addition of new mechanisms discussed in Section 3.2). In the preexisting MCM, the fractions to form phenoxy-like radicals (i.e., C_6H_5O and oxygen-centered radical of catechol) via the OH-abstraction reaction of phenols (-O-H) range from 0.06 to 1. When these preexisting fractions in the current MCM mechanisms are employed, the gas simulation shown in Fig. 2A and B is significantly deviated from observations due to an extraordinarily fast reactivity of phenoxy radicals with ozone as seen in Eqs. (1)–(3) (Tao and Li, 1999). The ozone formation in both phenols is almost negligible and the decay of phenols are underpredicted, and the conversion of NO to NO_2 is slow down.

Fig. 2C and B show the simulation with updated gas mechanisms for the branch ratio to form phenoxy radical (0.06 to 0.01) and newly added low volatility products as described in Section 3.2. Except NO_2, the consumption of both phenols and the concentrations of NO and ozone were reasonably predicted. When the phenoxy radical formation is excluded from the mechanism and new mechanisms in Figs. S2 and S3 are added, a remarkable improvement in the ozone prediction appears as seen in Fig. 2.

However, the gas simulation of both phenols in the presence of SA seed aerosol is largely deviated from observation as seen in Fig. 2E and F suggesting the formation of phenoxy radicals via the heterogeneous reactions of phenols in acidic inorganic seed. The formation of phenoxy radicals have been reported in matrices at low temperatures (Sun et al., 1990), strong acids (Dixon and Murphy, 1976), or gas-phase clusters under specific conditions (Steadman and Syage, 1991). For example, the existence of phenoxy radicals has also been found in strong acidic solutions by measuring phenoxy radicals with Electron Spin Resonance (ESR) Spectroscopy (Dixon and Murphy, 1978). However, the formation of phenoxy radicals in previous studies has been mainly focused on condensed media.

In the gas phase, an OH radical react with an phenolic OH but is favored to undergo addition directly to an aromatic ring (Figs. S2 and S3) (Berndt and Böge, 2003). The results of this study suggest that the formation of a phenoxy radical from the phenol dissolved in wet-seed aerosol is more affordable than in gas phase by the two possible mechanisms. Firstly, the hydrophilic phenol partitioned to salted aqueous media reacts with the OH radical (aq) in the similar way with the OH addition to the aromatic ring in the gas phase to form an OH-added intermediate phenol ($HO\text{-}C_6H_5^{\bullet}OH$, Eqs. R1–R10 of Section S4). Unlike the gas phase, the $HO\text{-}C_6H_5^{\bullet}OH$ radical form the phenoxy radical via the loss of a water molecule (R11-R12) (Das, 2005; Mvula et al., 2001; Singh et al., 2009), instead of reacting with an oxygen molecule. Various oxidants including OH, HO_2, and ozone are available in air and can be partitioned into the aqueous phase (Eqs. R1–R8), where they are attributed to oxidation of organic species. Secondly, a phenoxy radical can be directly formed though the irradiation

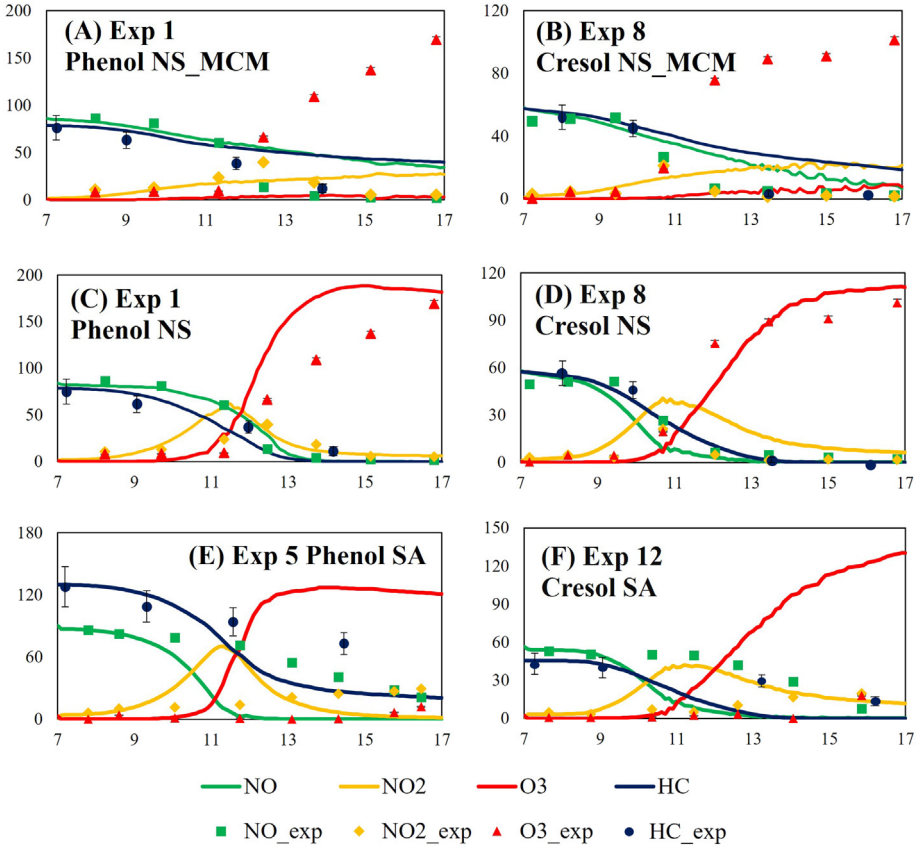

Fig. 2. The time profiles of observations and the prediction for concentrations of NO, NO_2, and O_3 and phenolic compounds (Table 1). "Phenol NS_MCM" demotes the gas simulation of phenols with the original MCM (version 3.3.1) in the absence of inorganic seed. "Phenol NS" and "Phenol SA" denote the gas simulation of phenols with the modified MCM based on the description in Section 3.2 in the absence and presence of SA seed, respectively. The concentrations of phenol or *o*-cresol were measured by using UV spectral data as described in Section 2.1. The error associated with NO, NO_2, and O_3 are 2 % and not visible in this Figure. The error associated with the concentration of phenol measured with UV spectrometry is 15 %.

of phenol under UV light in strongly acidic media (Eqs. R13–R14) (Siano et al., 2020). The phenoxy radical formed in the aqueous aerosol phase is then evaporate into the gas phase to interrupt atmospheric chemistry of ozone and retard further phenol oxidation (Eqs. (1)–(4)). In this study, phenoxy radicals are not limited to phenol and *o*-cresol and include multifunctional phenoxy radicals originating from their oxygenated products.

In order to search the evidence of the impact of SA seed on the formation of phenoxy radicals, the mass fragmentation peaks obtained from ACSM data were analyzed. Fig. 3 illustrates the mass ratio of a phenoxy radical to a phenol associated with catechol and methyl catechol, which are the dominant first-generation oxidation products of phenol and *o*-cresol, respectively (Figs. S2 and S3). The phenoxy radicals originating from catechol or methyl catechols are semivolatile and they can be shown in ACSM data, which measure the fragmentation pattern of aerosol products. The *m/z* peaks (M) of catechol and methyl catechol were 110 and 124, respectively in ACSM fragmentation spectra, and their m/z of phenoxy radicals appeared at 109 and 123, respectively. The fragmentations of both catechol and methyl catechol are dominated by M and thus, M-1 peaks can mainly originate from phenoxy radicals. The mass ratios of M-1 (phenoxy radicals) to M (phenols) of in SA-seeded SOA were significantly higher than those in non-seed SOA for both catechol or methyl catechol evidently. It is convincing that phenoxy radicals can interrupt atmospheric chemistry but their formation needs to be further studied with both heterogeneous chemistry of phenol in the presence of inorganic seed aerosol and the accurately determined branching ratio to form phenoxy radicals.

4.2. SOA simulation in the absence of inorganic aerosol

Fig. 4 shows chamber-generated SOA mass produced from the photooxidation of phenol and *o*-cresol in the absence of a salted aqueous phase (Table 1). In addition, Fig. 4 also illustrates the simulation of SOA mass using the UNIPAR model integrated with the preexisting MCM or the modified MCM mechanisms (Section 3.2 Gas Oxidation Mechanisms). A considerable improvement in predicting non-seed SOA mass appeared with both the branching ratio to form phenoxy radicals and the newly added path via peroxy radical adducts originating from the addition of an OH radical to phenols. The accurate prediction of the consumption of phenols is precondition to predict the concentration of phenol oxidation products and its SOA mass. The inclusion of low volatile products in the model increases the contribution of SOA originating from a partitioning process (OM_{P_mod} in Fig. 4). On average, 50 % of total SOA mass (OM_{T_mod}) is contributed by OM_{P_mod} for *o*-cresol and about 30 % of SOA mass for phenol in simulation with the modified gas mechanism. The fraction of OM_{P_mod} of OM_{T_mod} in

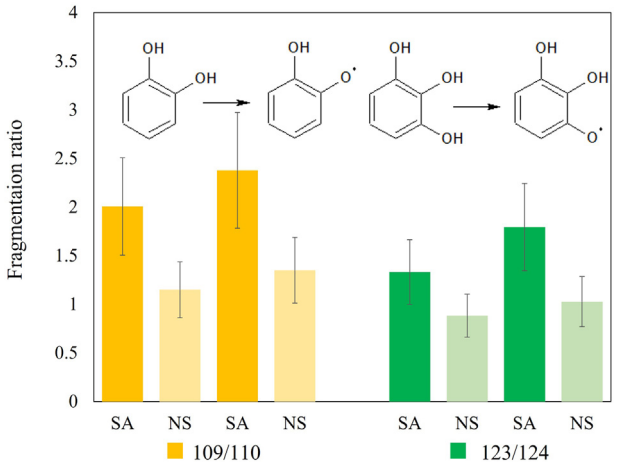

Fig. 3. The fragmentation ratios of catechol (109/110) observed in Exp. 2 and 5 for phenol oxidation and methyl catechol (123/124) observed in Exp. 9 and 13 for *o*-cresol oxidation. The error bars associated with fragmentation ratios are estimated with a propagation error estimation method using ACSM data.

phenolic SOA is much greater than that of conventional aromatic SOA (Han and Jang, 2020, 2022).

4.3. Effects of wet seed on phenolic SOA

Fig. 5 shows the simulated and observed SOA masses produced in the presence of SA or wet-AS seed (a and b for phenol; d and e for *o*-cresol). Remarkably, phenolic SOA formation was suppressed in the presence of acidic inorganic seed aerosol. This result suggests that persistence phenoxy radicals heterogeneously formed from phenol or *o*-cresol in wet-inorganic aerosol can influence SOA formation. The current UNIPAR model was able to well simulate non-seed SOA as demonstrated in Fig. 4 of Section 4.2, but the model has no feature to simulate heterogeneously formed phenoxy radical and its impact on SOA mass. In order to demonstrate the suppression of SOA formation due to wet inorganic seed, the SOA mass was simulated with the current UNIPAR model of this study at a given experimental condition (Table 1) and compared with chamber data.

Noticeably, the results in Fig. 5 are very different from the conventional impact of aerosol acidity on SOA formation. In general, SA is known to accelerate the formation of nonvolatile oligomeric matter via acid-catalyzed reactions of reactive organic compounds and increase SOA mass (Jang et al., 2002; Hallquist et al., 2009). Fig. 5 also includes the simulation of SOA mass in the absence of inorganic seed at given concentration of hydrocarbon and NO_x. The observed SOA mass (Fig. 5a, b, d, and e) in the presence of SA seed was even lower than the simulated non-seed SOA mass for both phenols clearly evincing that SA can suppress SOA formation. The wet-AS seed (Fig. 5c and f) also obstructs SOA formation, although to a lesser extent than SA. This study proposes that the formation of phenoxy radicals is heterogeneously processed in salted aqueous phase and significantly accelerated by aerosol acidity. The formation of phenoxy radicals have been reported in matrices at low temperatures (Sun et al., 1990), strong acids (Dixon and Murphy, 1976), or gas-phase clusters under specific conditions (Steadman and Syage, 1991). In general, acidic media are favorable to oxidize chemical species. For example, the formation of the phenoxy radical from intermediate product, HO-$C_6H_5^{\bullet}$OH radical (R11-R12), is accelerated by an acid catalyst (Das, 2005; Mvula et al., 2001; Singh et al., 2009). An electron in reactions R13 and R14 of Section S4 can react with H^+ in acidic media to form a hydrogen radical (Ghassemzadeh et al., 2013). This hydrogen radical initiates to form other oxidant radicals that can react with phenols to form phenoxy radicals.

In the presence of wet-AS seed, the phenolic SOA formation is not only influenced by heterogeneous chemistry of phenols in the inorganic aqueous phase, but it can also be impacted by heterogeneous reactions of reactive organic products to form oligomeric matter. Thus, a significant amount of SOA mass forms with wet-AS but its mass is somewhat overpredicted by the model (Fig. 5c and f) suggesting that SOA formation is still suppressed by phenoxy radicals.

4.4. Sensitivity of SOA formation to major variables and uncertainties to model parameters

The sensitivity of the UNIPAR-predicted SOA mass to temperature and different NO_x levels was evaluated at the given sunlight conditions (between 6:30 AM to5:30 PM EST on September 30, 2021). The consumption of HCs in each simulation was set to 20 ppb (4:00 PM EST). Therefore, the initial concentration of phenol or *o*-cresol is varied. The sensitivity test was limited to SOA formation in the absence of wet-inorganic seed to avoid suppression of ozone due to the heterogeneously formed phenoxy radical.

The SOA yield tends to increase with decreasing temperature from 298 K to 278 K (Fig. 6). SOA production increases because of lower vapor pressure at lower temperatures. Overall, *o*-cresol produces much higher SOA mass than phenol at given simulation conditions (same HC consumption, NO_x levels, and sunlight). The volatility of phenol oxidation products is generally higher than that of *o*-cresol. Thus, phenol SOA is more sensitive to temperature than *o*-cresol SOA. Additionally, phenol SOA is more sensitive to NO_x levels than cresol. The SOA yields of both phenol and *o*-cresol

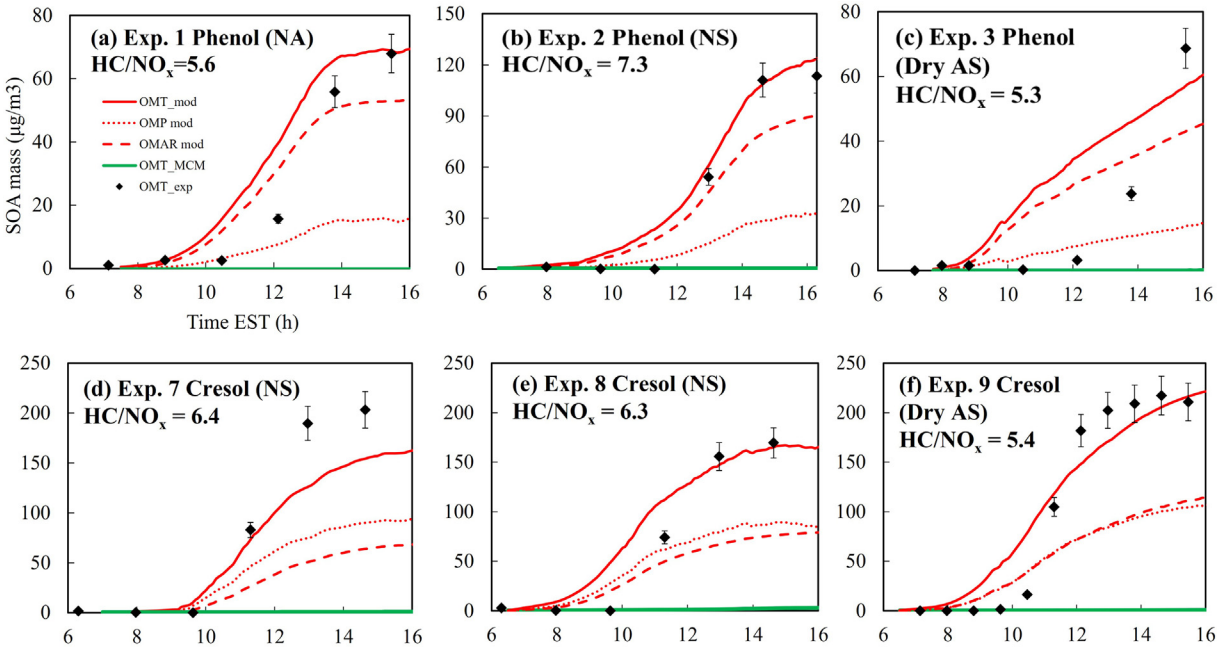

Fig. 4. The simulated SOA mass (solid line) and measure SOA mass (♦) in the absence of wet inorganic aerosol under different NO_x levels (Table 1). The SOA simulation with the UNIPAR model originating from the gas products in the preexisting MCM (green solid line) was compared with that simulated with the UNIPAR originating from the MCM modified by including peroxide moieties described in Section 3.2 (red solid line). The UNIPAR-predicted OM_{AR} (heterogeneous reactions in aerosol phase) and OM_p (partitioning) are also included. The error associated with SOA data was 9 % according to the uncertainty in OC/EC data.

rapidly increase as the HC/NO_x ratio increases up to 7 ppbC/ppb, then gradually decreases beyond 7 ppbC/ppb. At higher NO_x levels, more organonitrate (which is mainly controlled by the partitioning process) forms due to the reaction of peroxy radicals with NO. Thus, the OM_{AR} fraction of SOA mass drops with increasing the NO_x level causing higher sensitivity to NO_x levels in phenol than *o*-cresol. The OM_{AR} is higher in phenol SOA than cresol SOA as seen in Fig. 4.

For SOA mass simulation in the absence of salted inorganic aqueous aerosol, Fig. 7 demonstrates the impact of the important model parameters (vapor pressure (VP), aerosol phase reaction (k_o), and the newly added mechanisms) on SOA formation. All simulations were performed with the same amount of HC consumption (20 ppb) under the given sunlight profile on September 30, 2021. The variation of VP and k_o was determined with factors of 0.5 and 2. The uncertainty factors for the estimated VP were set

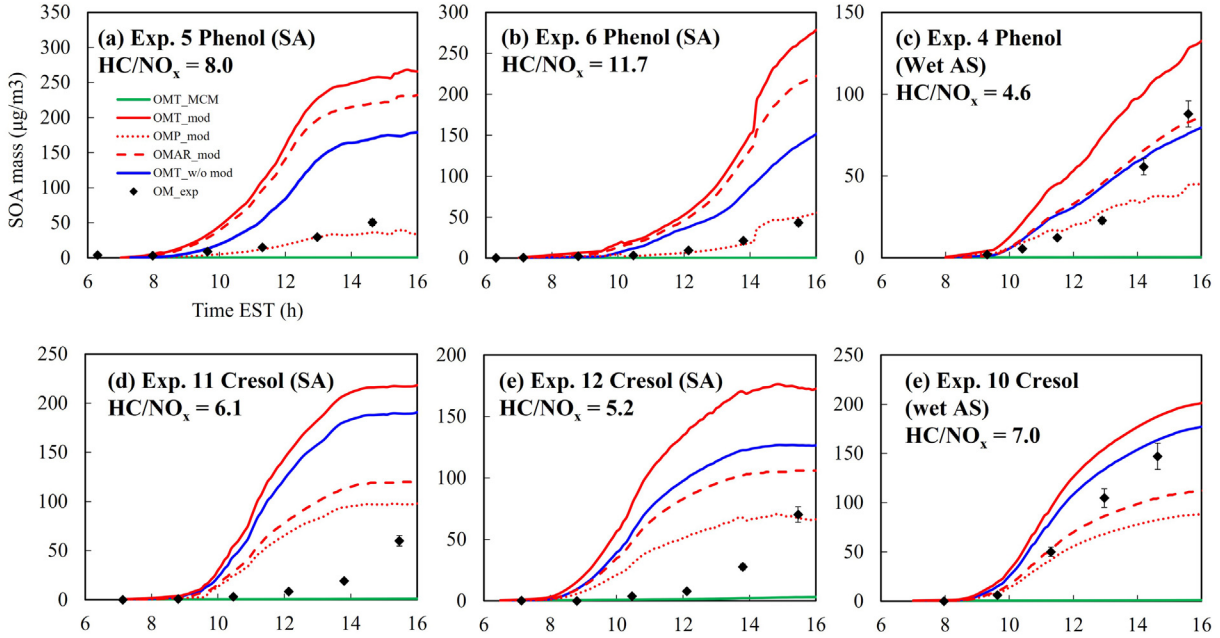

Fig. 5. The simulated SOA mass in the presence of SA or wet-AS (solid line) and measured SOA mass (♦) under different NO_x levels in the absence of SA or wet-AS (Table 1). The SOA mass simulated with the preexisting MCM (green solid line) was compared with that simulated with the MCM modified by including peroxide moieties (red solid line). The UNIPAR-predicted OM_{AR} (heterogeneous reaction in aerosol phase) and OM_p (partitioning) are also included. The error related to SOA data was 9 % according to the uncertainty in OC/EC data. For comparison, SOA mass was also predicted in the absence of seed aerosol (blue solid line).

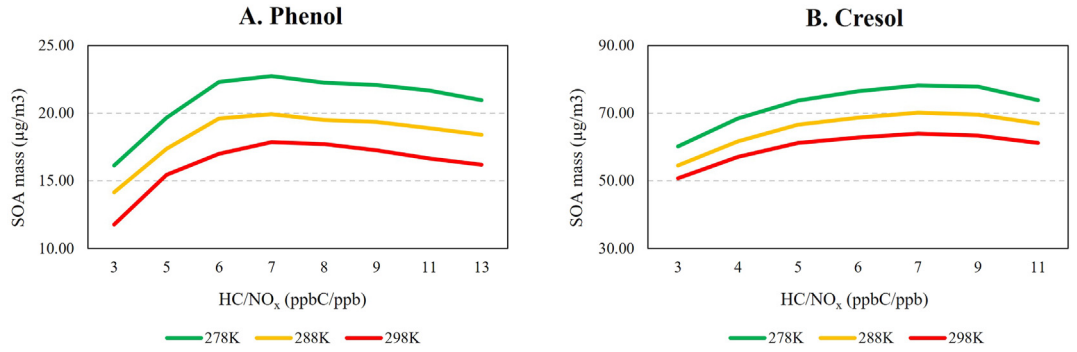

Fig. 6. The sensitivity of the predicted SOA mass to the model parameters (NO_x and temperature). Temperature levels were set to 298 K, 288 K, and 278 K. The NO_x levels (HC ppbC/NO_x ppb) range from 3 to 13. SOA simulations were performed at a given sunlight profile on September 30, 2021 (from 6:30 AM to 17:30, local time). The simulations were performed with 20 ppb consumption of HC.

based on the reported uncertainty associated with the group contribution method (Zhao et al., 1999; Yu et al., 2021b). The corresponding change in the SOA mass ranges from −9 % to 7 % in phenol SOA simulation, and from −7 % to 6 % in *o*-cresol SOA simulation. The uncertainties related to k_o is relatively small, ranging from −3 % to 2 % for phenol and − 2 % to 2 % for *o*-cresol.

The variation in SOA formation with the newly added gas oxidation mechanisms was significant. To simulate the impact of the new path, the fraction (f_{RO2}) leading to the formation of the non-bicyclic peroxy radical (Section 3.2, Figs. S2 and S3) increases from 0.1 to 0.2 or decreases from 0.1 to 0.05 at the two different NO_x levels in Fig. 7. With increasing f_{RO2} in the modified MCM, SOA mass of phenol increases 32 % and decreases 31 % at high NO_x and increases 54 % and decreases 29 % at low NO_x. For *o*-cresol, SOA mass increases 31 % and decreases 43 % at high NO_x and increases 21 % and decreases 46 % at low NO_x. This trend suggests that identification of missing gas mechanisms is important to accurately simulate phenolic SOA formation.

4.5. SOA compositions

The functional group compositions of phenol and *o*-cresol SOA in the absence and the presence of sulfuric acid aerosol were determined through decoupling of FTIR data. The curve fitting parameters for the FTIR peak include the center frequency, the peak absorbance, and the half width at half-height. The band shape in the FTIR spectra was approximated by a Gaussian shape (Jang and Kamens, 2001; Griffiths and De Haseth, 2007). The relative functional group intensities for —OH, —COOH, —C═C, C—O, C═O and —NO_2 were normalized with that of C—H stretching. Although SOA yields decreased in the presence of SA, the impact of acid-catalyzed reactions can still be observed. For example, carbonyl peaks in SA-seeded SOA appeared smaller compared to non-seeded SOA, and C—O stretching (excluding carboxylic acid and alcohol C—O stretching) in SA-seeded SOA was increased due to the formation of acetals and hemiacetals from oligomers (Jang et al., 2002; Jang and Kamens, 2001; Yu et al., 2021b).

The FTIR functional group compositions in the absence of SA were also compared with the model predicted compositions as seen in Fig. 8. Overall, the observed compositions were predicted by the model. In the absence of seed aerosol, the O:C ratios of both phenol and *o*-cresol estimated with FTIR functional group contributions were 0.93 ± 0.09 and 0.94 ± 0.09, respectively. The UNIPAR-predicted O:C ratios of non-seed SOA for phenol and *o*-cresol are 0.9 and 0.93, respectively, and they accord well with observed values. The reported O:C ratio of the SOA produced via the photooxidation of phenol with H_2O_2 (Sun et al., 2010; Yu et al., 2014) ranges from 1.06 to1.23. Yee et al. reported an O:C ratio of 0.88 ± 0.27 for the phenol SOA produced under the low NO_x level (Chhabra et al., 2011; Yee et al., 2013). In the presence of SA, the O:C ratios of phenol and *o*-cresol decreased to 0.72 ± 0.07 and 0.78 ± 0.08, respectively. The possible explanation for such reduction in SA-seeded SOA can be the retardation of the oxidation of phenolic compounds due to the formation of persistent phenoxy radicals as discussed in Section 4.1.

5. Atmospheric implications

In general, the smoldering condition during biomass burning emits low NO_x compared to fuel combustion at high temperatures (Simoneit, 2002; Buhre et al., 2005; Mebust and Cohen, 2013). To date, wildfire smoke is known to contribute to ozone increase in urban environments. However, its impact on atmospheric chemistry is still poorly understood, particularly when wildfire smoke is blended with NO_x and other anthropogenic pollutants in urban areas. The UNIPAR model employed in this study predicts

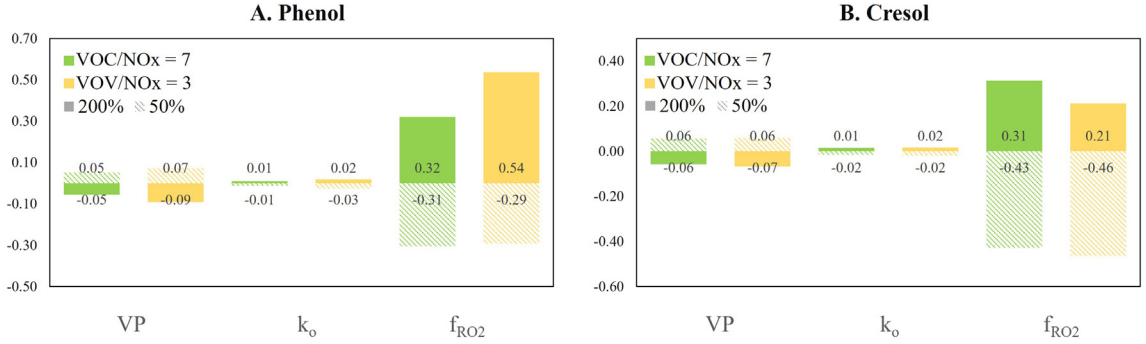

Fig. 7. The uncertainty test of the predicted SOA mass due to major model parameters: vapor pressure (VP), reaction rate constant in the organic phase (k_o), and reaction fraction to form non-bicyclic peroxy radical formation mechanism (f_{RO2}). The uncertainty was estimated by increasing and decreasing parameters by 200 % or 50 %. All simulations of phenol and *o*-cresol were performed under the given reference meteorological profiles on September 30, 2021, with 20 ppb HC consumption.

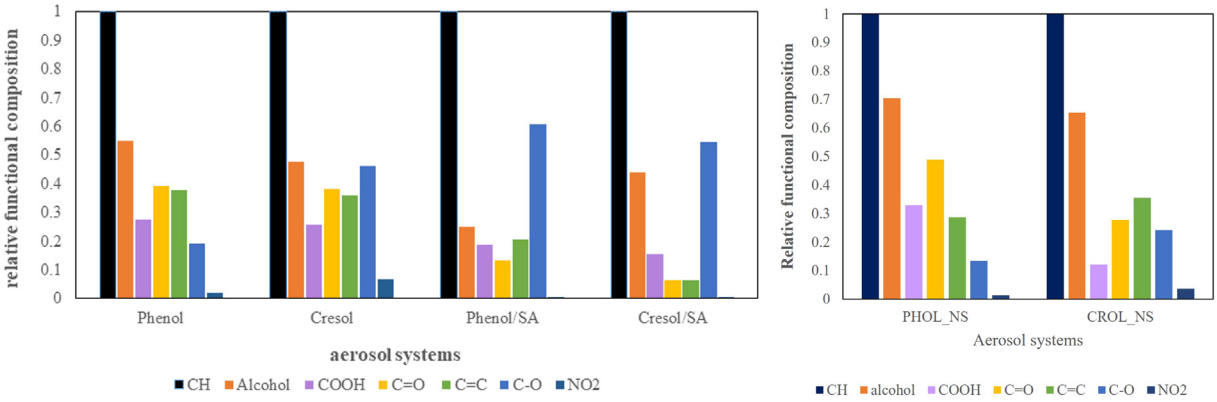

Fig. 8. (a) Relative functional group compositions constructed by using FTIR data for phenol SOA and *o*-cresol SOA under two different seed conditions (non-seed and sulfuric acid). NS and SA refers to non-seed and sulfuric acid, respectively. The y-axis shows the relative intensity of functional groups normalized with the C—H stretching. Phenol SOA data was collected on September 30, 2021, and *o*-cresol SOA data was collected on October 14, 2021 (Table 1). (b) Relative functional group compositions constructed by using UNIPAR simulation results in the absence of seed aerosol.

well the SOA formation from phenol and *o*-cresol in the absence of wet-inorganic seed under varying NO_x levels and this model can improve the prediction of atmospheric chemistry of biomass burning smoke gases in urban air. The model prediction suggests that phenolic SOA forms through both gas-aerosol partitioning of low-volatility products and oligomeric matter from heterogeneous reactions of reactive organic species. Generally, the impact of NO_x on phenol SOA and *o*-cresol SOA follows the trends seen in typical SOA from various HCs such as aromatics, isoprene, and terpene (Zhou et al., 2019; Beardsley and Jang, 2016; Yu et al., 2021b), showing an increase in SOA yields with decreasing NO_x. The model simulation suggested that phenol SOA was also more sensitive to either temperature or NO_x than *o*-cresol SOA. The insensitivity of *o*-cresol can be explained due to the greater fraction of very lowly-volatile products in *o*-cresol than that in phenol SOA.

Unexpectedly, the observed ozone (Fig. 2) and phenolic SOA formation (Fig. 5) were suppressed in the presence of SA seed and wet-AS seed. This result proposed that phenolic radicals can be generated via heterogeneous chemistry of phenols and influence phenolic SOA formation. In particular, strongly acidic SA aerosol can significantly impact this new pathway. The role of aerosol acidity on phenolic SOA formation is contradicted with the traditional view on the acceleration of SOA growth by SA aerosol (Jang et al., 2002; Hallquist et al., 2009). The current UNIPAR model has no mechanism to simulate heterogeneous chemistry of the phenoxy radical formation in the presence of wet inorganic seed. Although the UNIPAR model is capable of simulating SOA formation via multiphase reactions of various HCs in the presence of electrolytic inorganic aerosol, it fails to predict phenolic SOA mass in this study due to heterogeneously formed persistent phenoxy radicals. The chamber-generated SOA mass was far deviated from simulated SOA mass with the current UNIPAR model of this study at given experimental conditions. The results from this study suggest that persistent phenoxy radicals produced during wildfire episodes can retard the atmospheric oxidation rate and possibly produce less SOA compared to laboratory studies. In general, phenols are oxidized with the OH radical produced by photolysis of the high concentration of H_2O_2 and HONO (Nakao et al., 2011; Nakao et al., 2013; Yu et al., 2014; Yee et al., 2013; Sun et al., 2010) in the absence of wet-inorganic seed, which is very different from ambient air.

The chemical constituents of biomass burning smoke vary depending upon the type of vegetation (Lewis et al., 2009). For instance, inorganic matter such as potassium, chloride, sulfate, and trace minerals usually comprise 12–24 % of particulate mass produced from biomass burning (Reid et al., 2005; Yokelson et al., 2009; Hodshire et al., 2019). Furthermore, studies have shown that inorganic secondary species can increase up to 3 to 5 times in aged smoke (Reid et al., 1998; Formenti et al., 2003). The wet aerosol originating from both primary and secondary inorganic electrolytes can potentially promote the formation of phenoxy radicals. Consequently, the resulting persistent phenoxy radicals intervene with the ozone path of OH radical formation and delay HC oxidation and SOA formation.

Several unresolved issues need to be improved to accurately predict SOA formation from biomass burning, including gas mechanisms, the role of the aqueous phase on the formation of phenoxy radicals, and SOA formation from wildfire smoke gases other than phenol and *o*-cresol. The current MCM uses near explicit oxidation chemistry for HC gases. However, there are still missing mechanisms, including cross-reactions of RO_2 radicals and the distribution of oxidation paths as discussed in Section 3.2. The result of this study suggests the necessity of new insights to simulate phenols' unique characteristics to form SOA and ozone in the presence of electrolytic salt aerosol under the urban and rural sets. In addition, numerous HCs are contained in wildfire smoke gas, although phenol and *o*-cresol of this study are frequently found. For example, an in-depth study of the SOA formation from methoxy-phenols (Bruns et al., 2016) is needed in the future.

Additionally, the comprehension of the atmospheric process of phenolic compounds like phenol and cresols is essential for better prediction of SOA formation from major aromatic HCs. For example, phenol is the most abundant first-generation product from the oxidation of benzene and attributes to 53 % of OH-initiated reactions (Smith et al., 2014; Johnson et al., 2005). Cresol is involved in 18 % of toluene-OH reactions. Xu et al. explained that toluene SOA formation was underestimated by about 20 % (Xu et al., 2015). Studies (Schmitt, 2018; Garmash et al., 2020) suggest that highly oxygenated molecules form during benzene oxidation and the absence of these products results in a significant underestimation of benzene SOA (up to 50 %). The addition of improved oxidation mechanisms of phenol and *o*-cresol to the MCM can also improve toluene and benzene gas mechanisms and the prediction of SOA formation.

CRediT authorship contribution statement

Choi performed chamber experiments, processed experimental data, and simulated SOA formation using the UNIPAR model. Jang performed chamber experiments, assisted data processes, and developed the SOA model.

Data availability

Data will be made available on request.

Declaration of competing interest

There is no any financial and personal relationship with other people or organizations to publish this paper.

Acknowledgments

This research was supported by the National Institute of Environmental Research (NIER2020-01-01-010), the National Science Foundation (AGS1923651), and the Fine Particle Research Initiative in East Asia Considering National Differences (FRIEND) Project through the National Research Foundation of Korea (NRF) funded by the Ministry of Science and ICT (2020M3G1A1114556).

Appendix A. Supplementary data

Supplementary data to this article can be found online at https://doi.org/10.1016/j.scitotenv.2022.158082.

References

Akherati, A., He, Y., Coggon, M.M., Koss, A.R., Hodshire, A.L., Sekimoto, K., Warneke, C., De Gouw, J., Yee, L., Seinfeld, J.H., 2020. Oxygenated aromatic compounds are important precursors of secondary organic aerosol in biomass-burning emissions. Environ. Sci. Technol. 54, 8568–8579.

Atkinson, R., 2000. Atmospheric chemistry of VOCs and NOx. Atmos. Environ. 34, 2063–2101.

Barsanti, K.C., Kroll, J.H., Thornton, J.A., 2017. Formation of low-volatility organic compounds in the atmosphere: recent advancements and insights. J. Phys. Chem. Lett. 8, 1503–1511.

Beardsley, R.L., Jang, M., 2016. Simulating the SOA formation of isoprene from partitioning and aerosol phase reactions in the presence of inorganics. Atmos. Chem. Phys. 16, 5993–6009.

Beardsley, R., Jang, M., Ori, B., Im, Y., Delcomyn, C.A., Witherspoon, N., 2013. Role of sea salt aerosols in the formation of aromatic secondary organic aerosol: yields and hygroscopic properties. Environ. Chem. 10, 167–177.

Berndt, T., Böge, O., 2003. Gas-phase reaction of OH radicals with phenol. Phys. Chem. Chem. Phys. 5, 342–350.

Bruns, E.A., El Haddad, I., Slowik, J.G., Kilic, D., Klein, F., Baltensperger, U., Prévôt, A.S., 2016. Identification of significant precursor gases of secondary organic aerosols from residential wood combustion. Sci. Rep. 6, 1–9.

Buhre, B.J., Elliott, L.K., Sheng, C., Gupta, R.P., Wall, T.F., 2005. Oxy-fuel combustion technology for coal-fired power generation. Prog. Energy Combust. Sci. 31, 283–307.

Calvert, J.G., Atkinson, R., Becker, K.H., Kamens, R.M., Seinfeld, J.H., Wallington, T.H., Yarwood, G., 2002. The Mechanisms of Atmospheric Oxidation of the Aromatic Hydrocarbons.

Capes, G., Johnson, B., McFiggans, G., Williams, P., Haywood, J., Coe, H., 2008. Aging of biomass burning aerosols over West Africa: aircraft measurements of chemical composition, microphysical properties, and emission ratios. J. Geophys. Res. Atmos. 113.

Carter, W.P., Atkinson, R., 1989. Alkyl nitrate formation from the atmospheric photoxidation of alkanes; a revised estimation method. J. Atmos. Chem. 8, 165–173.

Carter, W.P., Heo, G., Cocker III, D.R., Nakao, S., 2012. SOA Formation: Chamber Study and Model Development, Final Report to CARB Contract, 08-326.

Chen, J., Li, C., Ristovski, Z., Milic, A., Gu, Y., Islam, M.S., Wang, S., Hao, J., Zhang, H., He, C., 2017. A review of biomass burning: emissions and impacts on air quality, health and climate in China. Sci. Total Environ. 579, 1000–1034.

Chhabra, P., Ng, N., Canagaratna, M., Corrigan, A., Russell, L., Worsnop, D., Flagan, R., Seinfeld, J., 2011. Elemental composition and oxidation of chamber organic aerosol. Atmos. Chem. Phys. 11, 8827–8845.

Cohen, A.J., Brauer, M., Burnett, R., Anderson, H.R., Frostad, J., Estep, K., Balakrishnan, K., Brunekreef, B., Dandona, L., Dandona, R., 2017. Estimates and 25-year trends of the global burden of disease attributable to ambient air pollution: an analysis of data from the global burden of diseases study 2015. Lancet 389, 1907–1918.

Das, T.N., 2005. Oxidation of phenol in aqueous acid: characterization and reactions of radical cations Vis-à-Vis the phenoxyl radical. J. Phys. Chem. A 109, 3344–3351.

Dixon, W.T., Murphy, D., 1976. Determination of the acidity constants of some phenol radical cations by means of electron spin resonance. J. Chem. Soc., Faraday Trans. 2 72, 1221–1230.

Dixon, W.T., Murphy, D., 1978. Determination of acid dissociation constants of some phenol radical cations. J. Chem. Soc., Faraday Trans. 2 74, 432–439.

Docherty, K.S., Stone, E.A., Ulbrich, I.M., DeCarlo, P.F., Snyder, D.C., Schauer, J.J., Peltier, R.E., Weber, R.J., Murphy, S.M., Seinfeld, J.H., 2008. Apportionment of primary and secondary organic aerosols in Southern California during the 2005 study of organic aerosols in Riverside (SOAR-1). Environ. Sci. Technol. 42, 7655–7662.

Donahue, N.M., Robinson, A., Stanier, C., Pandis, S., 2006. Coupled partitioning, dilution, and chemical aging of semivolatile organics. Environ. Sci. Technol. 40, 2635–2643.

Donahue, N.M., Henry, K.M., Mentel, T.F., Kiendler-Scharr, A., Spindler, C., Bohn, B., Brauers, T., Dorn, H.P., Fuchs, H., Tillmann, R., 2012. Aging of biogenic secondary organic aerosol via gas-phase OH radical reactions. Proc. Natl. Acad. Sci. 109, 13503–13508.

Finlayson-Pitts, B.J., Pitts Jr., J.N., 1999. Chemistry of the Upper and Lower Atmosphere: Theory, Experiments, and Applications. Elsevier.

Formenti, P., Elbert, W., Maenhaut, W., Haywood, J., Osborne, S., Andreae, M., 2003. Inorganic and carbonaceous aerosols during the Southern African Regional Science Initiative (SAFARI 2000) experiment: chemical characteristics, physical properties, and emission data for smoke from African biomass burning. J. Geophys. Res. Atmos. 108.

Garmash, O., Rissanen, M.P., Pullinen, I., Schmitt, S., Kausiala, O., Tillmann, R., Zhao, D., Percival, C., Bannan, T.J., Priestley, M., 2020. Multi-generation OH oxidation as a source for highly oxygenated organic molecules from aromatics. Atmos. Chem. Phys. 20, 515–537.

Ghassemzadeh, L., Peckham, T.J., Weissbach, T., Luo, X., Holdcroft, S., 2013. Selective formation of hydrogen and hydroxyl radicals by electron beam irradiation and their reactivity with perfluorosulfonated acid ionomer. J. Am. Chem. Soc. 135, 15923–15932.

Griffiths, P.R., De Haseth, J.A., 2007. Fourier Transform Infrared Spectrometry. John Wiley & Sons.

Hallquist, M., Wenger, J.C., Baltensperger, U., Rudich, Y., Simpson, D., Claeys, M., Dommen, J., Donahue, N., George, C., Goldstein, A., 2009. The formation, properties and impact of secondary organic aerosol: current and emerging issues. Atmos. Chem. Phys. 9, 5155–5236.

Han, S., Jang, M., 2020. Simulating the impact of gas-wall partitioning on SOA formation using the explicit gas mechanism integrated with aqueous reactions containing electrolytes. Sci. Total Environ. 748, 141360.

Han, S., Jang, M., 2022. Prediction of secondary organic aerosol from the multiphase reaction of gasoline vapor by using volatility–reactivity base lumping. Atmos. Chem. Phys. 22, 625–639.

Hansch, C., McKarns, S.C., Smith, C.J., Doolittle, D.J., 2000. Comparative QSAR evidence for a free-radical mechanism of phenol-induced toxicity. Chem. Biol. Interact. 127, 61–72.

Hodshire, A.L., Akherati, A., Alvarado, M.J., Brown-Steiner, B., Jathar, S.H., Jimenez, J.L., Kreidenweis, S.M., Lonsdale, C.R., Onasch, T.B., Ortega, A.M., 2019. Aging effects on biomass burning aerosol mass and composition: a critical review of field and laboratory studies. Environ. Sci. Technol. 53, 10007–10022.

Im, Y., Jang, M., Beardsley, R., 2014. Simulation of aromatic SOA formation using the lumping model integrated with explicit gas-phase kinetic mechanisms and aerosol-phase reactions. Atmos. Chem. Phys. 14, 4013–4027.

Jang, M., Kamens, R.M., 2001. Atmospheric secondary aerosol formation by heterogeneous reactions of aldehydes in the presence of a sulfuric acid aerosol catalyst. Environ. Sci. Technol. 35, 4758–4766.

Jang, M., Czoschke, N.M., Lee, S., Kamens, R.M., 2002. Heterogeneous atmospheric aerosol production by acid-catalyzed particle-phase reactions. Science 298, 814–817.

Jang, M., Cao, G., Paul, J., 2008. Colorimetric particle acidity analysis of secondary organic aerosol coating on submicron acidic aerosols. Aerosol Sci. Technol. 42, 409–420.

Jenkin, M.E., Valorso, R., Aumont, B., Rickard, A.R., Wallington, T.J., 2018. Estimation of rate coefficients and branching ratios for gas-phase reactions of OH with aromatic organic compounds for use in automated mechanism construction. Atmos. Chem. Phys. 18, 9329–9349.

Jethva, H.T., Chand, D., Torres, O., Gupta, P., Lyapustin, A., Patadia, F., 2018. Agricultural burning and air quality over northern India: a synergistic analysis using NASA's A-train satellite data and ground measurements. Aerosol Air Qual. Res. 18.

Ji, Y., Zhao, J., Terazono, H., Misawa, K., Levitt, N.P., Li, Y., Lin, Y., Peng, J., Wang, Y., Duan, L., 2017. Reassessing the atmospheric oxidation mechanism of toluene. Proc. Natl. Acad. Sci. 114, 8169–8174.

Jimenez, J.L., Canagaratna, M., Donahue, N., Prevot, A., Zhang, Q., Kroll, J.H., DeCarlo, P.F., Allan, J.D., Coe, H., Ng, N., 2009. Evolution of organic aerosols in the atmosphere. Science 326, 1525–1529.

Johnson, D., Jenkin, M.E., Wirtz, K., Martin-Reviejo, M., 2005. Simulating the formation of secondary organic aerosol from the photooxidation of aromatic hydrocarbons. Environ. Chem. 2, 35–48.

Johnson, B., Osborne, S., Haywood, J., Harrison, M., 2008. Aircraft measurements of biomass burning aerosol over West Africa during DABEX. J. Geophys. Res. Atmos. 113.

Jolly, W.M., Cochrane, M.A., Freeborn, P.H., Holden, Z.A., Brown, T.J., Williamson, G.J., Bowman, D.M., 2015. Climate-induced variations in global wildfire danger from 1979 to 2013. Nat. Commun. 6, 1–11.

Kelly, J.M., Doherty, R.M., O'Connor, F.M., Mann, G.W., 2018. The impact of biogenic, anthropogenic, and biomass burning volatile organic compound emissions on regional and seasonal variations in secondary organic aerosol. Atmos. Chem. Phys. 18, 7393–7422.

Kleindienst, T.E., Jaoui, M., Lewandowski, M., Offenberg, J.H., Lewis, C.W., Bhave, P.V., Edney, E.O., 2007. Estimates of the contributions of biogenic and anthropogenic hydrocarbons to secondary organic aerosol at a southeastern US location. Atmos. Environ. 41, 8288–8300.

Kwok, E.S., Atkinson, R., 1995. Estimation of hydroxyl radical reaction rate constants for gas-phase organic compounds using a structure-reactivity relationship: an update. Atmos. Environ. 29, 1685–1695.

Laskin, J., Laskin, A., Nizkorodov, S.A., 2018. Mass spectrometry analysis in atmospheric chemistry. Anal. Chem. 90, 166–189.

Lewis, K., Arnott, W., Moosmüller, H., Chakrabarty, R., Carrico, C., Kreidenweis, S., Day, D., Malm, W., Laskin, A., Jimenez, J., 2009. Reduction in biomass burning aerosol light absorption upon humidification: roles of inorganically-induced hygroscopicity, particle collapse, and photoacoustic heat and mass transfer. Atmos. Chem. Phys. 9, 8949–8966.

Li, J., Jang, M., 2012. Aerosol acidity measurement using colorimetry coupled with a reflectance UV-visible spectrometer. Aerosol Sci. Technol. 46, 833–842.

Li, J., Jang, M., Beardsley, R.L., 2015. Dialkylsulfate formation in sulfuric acid-seeded secondary organic aerosol produced using an outdoor chamber under natural sunlight. Environ. Chem. 13, 590–601.

Lindenmayer, D.B., Taylor, C., 2020. New spatial analyses of australian wildfires highlight the need for new fire, resource, and conservation policies. Proc. Natl. Acad. Sci. 117, 12481–12485.

Majdi, M., Sartelet, K., Lanzafame, G.M., Couvidat, F., Kim, Y., Chrit, M., Turquety, S., 2019. Precursors and formation of secondary organic aerosols from wildfires in the Euro-Mediterranean region. Atmos. Chem. Phys. 19, 5543–5569.

Mancilla, Y., Herckes, P., Fraser, M.P., Mendoza, A., 2015. Secondary organic aerosol contributions to PM2. 5 in Monterrey, Mexico: temporal and seasonal variation. Atmos. Res. 153, 348–359.

Matsumi, Y., Kawasaki, M., 2003. Photolysis of atmospheric ozone in the ultraviolet region. Chem. Rev. 103, 4767–4782.
May, A., Lee, T., McMeeking, G., Akagi, S., Sullivan, A., Urbanski, S., Yokelson, R., Kreidenweis, S., 2015. Observations and analysis of organic aerosol evolution in some prescribed fire smoke plumes. Atmos. Chem. Phys. 15, 6323–6335.
Mebust, A.K., Cohen, R.C., 2013. Observations of a seasonal cycle in NOx emissions from fires in african woody savannas. Geophys. Res. Lett. 40, 1451–1455.
Mvula, E., Schuchmann, M.N., von Sonntag, C., 2001. Reactions of phenol-OH-adduct radicals. Phenoxyl radical formation by water elimination vs. oxidation by dioxygen. J. Chem. Soc., Perkin Trans. 2 264–268.
Nakao, S., Clark, C., Tang, P., Sato, K., Cocker Iii, D., 2011. Secondary organic aerosol formation from phenolic compounds in the absence of NO x. Atmos. Chem. Phys. 11, 10649–10660.
Nakao, S., Tang, P., Tang, X., Clark, C.H., Qi, L., Seo, E., Asa-Awuku, A., Cocker III, D., 2013. Density and elemental ratios of secondary organic aerosol: application of a density prediction method. Atmos. Environ. 68, 273–277.
Ng, N., Kroll, J., Chan, A., Chhabra, P., Flagan, R., Seinfeld, J., 2007. Secondary organic aerosol formation from m-xylene, toluene, and benzene. Atmos. Chem. Phys. 7, 3909–3922.
Odum, J.R., Hoffmann, T., Bowman, F., Collins, D., Flagan, R.C., Seinfeld, J.H., 1996. Gas/particle partitioning and secondary organic aerosol yields. Environ. Sci. Technol. 30, 2580–2585.
Olmez-Hanci, T., Arslan-Alaton, I., 2013. Comparison of sulfate and hydroxyl radical based advanced oxidation of phenol. Chem. Eng. J. 224, 10–16.
Permadi, D.A., Oanh, N.T.K., 2013. Assessment of biomass open burning emissions in Indonesia and potential climate forcing impact. Atmos. Environ. 78, 250–258.
Pillar-Little, E.A., Zhou, R., Guzman, M.I., 2015. Heterogeneous oxidation of catechol. J. Phys. Chem. A 119, 10349–10359.
Platz, J., Nielsen, O., Wallington, T., Ball, J., Hurley, M., Straccia, A., Schneider, W., Sehested, J., 1998. Atmospheric chemistry of the phenoxy radical, C6H5O (•): UV spectrum and kinetics of its reaction with NO, NO2, and O2. J. Phys. Chem. A 102, 7964–7974.
Pope Iii, C.A., Burnett, R.T., Thun, M.J., Calle, E.E., Krewski, D., Ito, K., Thurston, G.D., 2002. Lung cancer, cardiopulmonary mortality, and long-term exposure to fine particulate air pollution. JAMA 287, 1132–1141.
Reid, J.S., Hobbs, P.V., Ferek, R.J., Blake, D.R., Martins, J.V., Dunlap, M.R., Liousse, C., 1998. Physical, chemical, and optical properties of regional hazes dominated by smoke in Brazil. J. Geophys. Res. Atmos. 103, 32059–32080.
Reid, J., Koppmann, R., Eck, T., Eleuterio, D., 2005. A review of biomass burning emissions part II: intensive physical properties of biomass burning particles. Atmos. Chem. Phys. 5, 799–825.
Schmitt, S., 2018. Formation of Secondary Organic Aerosol from Photo-Oxidation of Benzene: A Chamber Study.
Schwantes, R.H., Schilling, K.A., McVay, R.C., Lignell, H., Coggon, M.M., Zhang, X., Wennberg, P.O., Seinfeld, J.H., 2017. Formation of highly oxygenated low-volatility products from cresol oxidation. Atmos. Chem. Phys. 17, 3453–3474.
Siano, G., Crespi, S., Bonesi, S.M., 2020. Direct irradiation of phenol and para-substituted phenols with a laser pulse (266 nm) in homogeneous and micro-heterogeneous media. A time-resolved spectroscopy study. J. Org. Chem. 85, 14012–14025.
Simoneit, B.R., 2002. Biomass burning—a review of organic tracers for smoke from incomplete combustion. Appl. Geochem. 17, 129–162.
Singh, U., Barik, A., Priyadarsini, K.I., 2009. Reactions of hydroxyl radical with bergenin, a natural poly phenol studied by pulse radiolysis. Bioorg. Med. Chem. 17, 6008–6014.
Smith, J.D., Sio, V., Yu, L., Zhang, Q., Anastasio, C., 2014. Secondary organic aerosol production from aqueous reactions of atmospheric phenols with an organic triplet excited state. Environ. Sci. Technol. 48, 1049–1057.
Spanget-Larsen, J., Gil, M., Gorski, A., Blake, D.M., Waluk, J., Radziszewski, J.G., 2001. Vibrations of the phenoxyl radical. J. Am. Chem. Soc. 123, 11253–11261.
Steadman, J., Syage, J.A., 1991. Picosecond studies of proton transfer in clusters. 2. Dynamics and energetics of solvated phenol cation. J. Am. Chem. Soc. 113, 6786–6795.
Steinfeld, J.I., 1998. Atmospheric chemistry and physics: from air pollution to climate change. Environ. Sci. Policy Sustain. Dev. 40 26-26.
Sun, Q., Tripathi, G., Schuler, R., 1990. Time-resolved resonance raman spectroscopy of p-aminophenol radical cation in aqueous solution. J. Phys. Chem. 94, 6273–6277.
Sun, Y., Zhang, Q., Anastasio, C., Sun, J., 2010. Insights into secondary organic aerosol formed via aqueous-phase reactions of phenolic compounds based on high resolution mass spectrometry. Atmos. Chem. Phys. 10, 4809–4822.
Surratt, J.D., Kroll, J.H., Kleindienst, T.E., Edney, E.O., Claeys, M., Sorooshian, A., Ng, N.L., Offenberg, J.H., Lewandowski, M., Jaoui, M., 2007. Evidence for organosulfates in secondary organic aerosol. Environ. Sci. Technol. 41, 517–527.
Tao, Z., Li, Z., 1999. A kinetics study on reactions of C6H5O with C6H5O and O3 at 298 K. Int. J. Chem. Kinet. 31, 65–72.
Tolocka, M.P., Jang, M., Ginter, J.M., Cox, F.J., Kamens, R.M., Johnston, M.V., 2004. Formation of oligomers in secondary organic aerosol. Environ. Sci. Technol. 38, 1428–1434.
Volkamer, R., Jimenez, J.L., San Martini, F., Dzepina, K., Zhang, Q., Salcedo, D., Molina, L.T., Worsnop, D.R., Molina, M.J., 2006. Secondary organic aerosol formation from anthropogenic air pollution: rapid and higher than expected. Geophys. Res. Lett. 33.
Wang, K., Zhang, Y., Yahya, K., Wu, S.-Y., Grell, G., 2015. Implementation and initial application of new chemistry-aerosol options in WRF/Chem for simulating secondary organic aerosols and aerosol indirect effects for regional air quality. Atmos. Environ. 115, 716–732.
Xu, J., Griffin, R.J., Liu, Y., Nakao, S., Cocker III, D.R., 2015. Simulated impact of NOx on SOA formation from oxidation of toluene and m-xylene. Atmos. Environ. 101, 217–225.
Yee, L., Kautzman, K., Loza, C., Schilling, K., Coggon, M., Chhabra, P., Chan, M., Chan, A., Hersey, S., Crounse, J., 2013. Secondary organic aerosol formation from biomass burning intermediates: phenol and methoxyphenols. Atmos. Chem. Phys. 13, 8019–8043.
Yevich, R., Logan, J.A., 2003. An assessment of biofuel use and burning of agricultural waste in the developing world. Glob. Biogeochem. Cycles 17.
Yokelson, R.J., Crounse, J., DeCarlo, P., Karl, T., Urbanski, S., Atlas, E., Campos, T., Shinozuka, Y., Kapustin, V., Clarke, A., 2009. Emissions from biomass burning in the Yucatan. Atmos. Chem. Phys. 9, 5785–5812.
Yu, L., Smith, J., Laskin, A., Anastasio, C., Laskin, J., Zhang, Q., 2014. Chemical characterization of SOA formed from aqueous-phase reactions of phenols with the triplet excited state of carbonyl and hydroxyl radical. Atmos. Chem. Phys. 14, 13801–13816.
Yu, L., Smith, J., Laskin, A., George, K.M., Anastasio, C., Laskin, J., Dillner, A.M., Zhang, Q., 2016. Molecular transformations of phenolic SOA during photochemical aging in the aqueous phase: competition among oligomerization, functionalization, and fragmentation. Atmos. Chem. Phys. 16, 4511–4527.
Yu, Z., Jang, M., Madhu, A., 2021a. Prediction of phase state of secondary organic aerosol internally mixed with aqueous inorganic salts. J. Phys. Chem. A 125, 10198–10206.
Yu, Z., Jang, M., Zhang, T., Madhu, A., Han, S., 2021b. Simulation of monoterpene SOA formation by multiphase reactions using explicit mechanisms. ACS Earth Space Chem. 5, 1455–1467.
Yu, Z., Jang, M., Kim, S., Son, K., Han, S., Madhu, A., Park, J., 2022. Secondary organic aerosol formation via multiphase reaction of hydrocarbons in urban atmospheres using CAMx integrated with the UNIPAR model. Atmos. Chem. Phys. 22, 9083–9098.
Zhang, Q., Jimenez, J.L., Canagaratna, M., Allan, J.D., Coe, H., Ulbrich, I., Alfarra, M., Takami, A., Middlebrook, A., Sun, Y., 2007. Ubiquity and dominance of oxygenated species in organic aerosols in anthropogenically-influenced northern hemisphere midlatitudes. Geophys. Res. Lett. 34.
Zhang, R., Wang, G., Guo, S., Zamora, M.L., Ying, Q., Lin, Y., Wang, W., Hu, M., Wang, Y., 2015. Formation of urban fine particulate matter. Chem. Rev. 115, 3803–3855.
Zhao, L., Li, P., Yalkowsky, S.H., 1999. Predicting the entropy of boiling for organic compounds. J. Chem. Inf. Comput. Sci. 39, 1112–1116.
Zhao, B., Wang, S., Donahue, N.M., Jathar, S.H., Huang, X., Wu, W., Hao, J., Robinson, A.L., 2016. Quantifying the effect of organic aerosol aging and intermediate-volatility emissions on regional-scale aerosol pollution in China. Sci. Rep. 6, 1–10.
Zhou, C., Jang, M., Yu, Z., 2019. Simulation of SOA formation from the photooxidation of monoalkylbenzenes in the presence of aqueous aerosols containing electrolytes under various NO x levels. Atmos. Chem. Phys. 19, 5719–5735.